AFRL-PR-WP-TP-2007-223

COOLING PERFORMANCE OF A PARTIALLY-CONFINED FC-72 SPRAY: THE EFFECT OF DISSOLVED AIR (POSTPRINT)

Rebekah L. Puterbaugh, Kirk L. Yerkes,
Travis E. Michalak, and Scott K. Thomas

JANUARY 2007

Approved for public release; distribution unlimited.

STINFO COPY

PROPULSION DIRECTORATE
AIR FORCE MATERIEL COMMAND
AIR FORCE RESEARCH LABORATORY
WRIGHT-PATTERSON AIR FORCE BASE, OH 45433-7251

REPORT DOCUMENTATION PAGE

Form Approved
OMB No. 0704-0188

1. REPORT DATE *(DD-MM-YY)*	2. REPORT TYPE	3. DATES COVERED *(From - To)*
January 2007	Conference Paper Postprint	07/01/2004 – 12/15/2006

4. TITLE AND SUBTITLE
COOLING PERFORMANCE OF A PARTIALLY-CONFINED FC-72 SPRAY: THE EFFECT OF DISSOLVED AIR (POSTPRINT)

5a. CONTRACT NUMBER
In-house

5b. GRANT NUMBER

5c. PROGRAM ELEMENT NUMBER
62203F

6. AUTHOR(S)
Rebekah L. Puterbaugh, Kirk L. Yerkes, and Travis E. Michalak (AFRL/PRPS)
Scott K. Thomas (Wright State University)

5d. PROJECT NUMBER
3145

5e. TASK NUMBER
20

5f. WORK UNIT NUMBER
C9

7. PERFORMING ORGANIZATION NAME(S) AND ADDRESS(ES)
Electrochemistry and Thermal Sciences Branch (AFRL/PRPS)
Power Division
Propulsion Directorate
Air Force Research Laboratory, Air Force Materiel Command
Wright-Patterson Air Force Base, OH 45433-7251

Wright State University
Department of Mechanical and Materials Engineering
Dayton, OH 45435

8. PERFORMING ORGANIZATION REPORT NUMBER
AFRL-PR-WP-TP-2007-223

9. SPONSORING/MONITORING AGENCY NAME(S) AND ADDRESS(ES)
Propulsion Directorate
Air Force Research Laboratory
Air Force Materiel Command
Wright-Patterson AFB, OH 45433-7251

10. SPONSORING/MONITORING AGENCY ACRONYM(S)
AFRL-PR-WP

11. SPONSORING/MONITORING AGENCY REPORT NUMBER(S)
AFRL-PR-WP-TP-2007-223

12. DISTRIBUTION/AVAILABILITY STATEMENT
Approved for public release; distribution unlimited.

13. SUPPLEMENTARY NOTES
Conference paper printed in the Proceedings of the 45th AIAA Aerospace Sciences Meeting and Exhibit, published by AIAA. This is a work of the U.S. Government and is not subject to copyright protection in the United States.

PAO Case Number: AFRL/WS 06-2899; Date cleared: 21 Dec 2006. This paper has color content.

14. ABSTRACT
This paper discusses the heat transfer performance of a partially-confined FC-72 spray with varying dissolved air concentrations. An experimental test rig was used to obtain critical heat flux (CHF) data. A nozzle allowed the fluid to be sprayed onto a thick-film resistor heater, which was mounted onto a glass post, with a sump system to allow removal of excess fluid. Type-E thermocouples were imbedded in the post to obtain temperature data. The parametric ranges for testing were: volume-percent concentration of dissolved air, 1 < C < 20%, chamber saturation pressure, 6.90E+4 < Psat < 8.27E+4 N/rn2, subcooling, 2 < DeltaTsc < 12 °C, volumetric flow rate, 6.31E-6 < V < 10.5E-6 rn3/s. Test data were obtained for comparison of CHF with varying C while controlling the spray chamber pressure. An empirical mathematical relationship allowing for determination of surface heat flux with varying flow rate was also developed. The model was obtained using test data at flow rates of V = 6.31E-6, 8.41E-6, and 1O.5E-6 m3/s, and was validated using experimental data obtained for flow rates of V = 7.36E-6 and 9.46E-6 m3/s.

15. SUBJECT TERMS
Thermal Management, Spray Cooling, Electronics Cooling, Dissolved Air

16. SECURITY CLASSIFICATION OF:			17. LIMITATION OF ABSTRACT:	18. NUMBER OF PAGES	19a. NAME OF RESPONSIBLE PERSON (Monitor)
a. REPORT	b. ABSTRACT	c. THIS PAGE			Kirk L. Yerkes
Unclassified	Unclassified	Unclassified	SAR	18	19b. TELEPHONE NUMBER *(Include Area Code)* N/A

Standard Form 298 (Rev. 8-98)
Prescribed by ANSI Std. Z39-18

45th AIAA Aerospace Sciences Meeting and Exhibit
8 - 11 January 2007, Reno, Nevada

AIAA 2007-199

Cooling Performance of a Partially-Confined FC-72 Spray: The Effect of Dissolved Air

Rebekah L. Puterbaugh*, Kirk L. Yerkes†, and Travis E. Michalak‡
Air Force Research Laboratory, Wright Patterson Air Force Base, Ohio, 45433

and

Scott K. Thomas§
Wright State University, Dayton, Ohio, 45435

The objective of this paper is to investigate the heat transfer performance of a partially-confined FC-72 spray with varying dissolved air concentrations. An experimental test rig consisting of a spray chamber coupled to a fluid delivery loop system was used to obtain critical heat flux (CHF) data. A spray downward nozzle, within the spray chamber, allowed the FC-72 fluid to be sprayed onto an upward facing, thick-film, resistor heater. The heater was mounted onto a glass post, with a sump system to allow removal of excess fluid. Type-E thermocouples were imbedded in the post to obtain temperature data. The parametric ranges for experimental testing were as follows: volume-percent concentration of dissolved air, $1 < C < 20\%$, chamber saturation pressure, $6.90\times10^4 \le P_{sat} \le 8.27\times10^4$ N/m^2 ($10 \le P_{sat} \le 12$ psia), subcooling, $2 \le \Delta T_{sc} \le 12$ °C, volumetric flow rate, $6.31\times10^{-6} \le \dot{V} \le 10.5\times10^{-6}$ m^3/s ($6.0 \le \dot{V} \le$ 10.0 gph). Test data were obtained for comparison of CHF with varying C while controlling the spray chamber pressure. An empirical mathematical relationship allowing for determination of surface heat flux with varying flow rate was also developed. The model was obtained using test data at flow rates of $\dot{V} = 6.31\times10^{-6}$, 8.41×10^{-6}, and 10.5×10^{-6} m^3/s (6.0, 8.0, and 10.0 gph), and was validated using experimental data obtained for flow rates of $\dot{V} = 7.36\times10^{-6}$ and 9.46×10^{-6} m^3/s (7.0 and 9.0 gph).

Nomenclature

C	=	% air content by volume, (volume fraction × 100 = [Vol_{air} / (Vol_{FC} + Vol_{air})] x 100)
C^*	=	air volume ratio, (Vol_{air} / Vol_{FC})
f	=	heater conduction loss fraction
H	=	thickness, m
k	=	thermal conductivity, W/(m-K)
M	=	molar fraction, (Mole_{air} / (Mole_{FC} + Mole_{air})
M^*	=	molar ratio, (Mole_{air} / Mole_{FC})
P	=	pressure, N/m^2
P_g	=	partial pressure, N/m^2
q	=	heat flux, W/m^2
Q	=	heat rate, W
T	=	temperature, °C
ΔT	=	T_s-T_{sat}, °C
ΔT_{sc}	=	fluid subcooling, °C
$\dot{V}$	=	volumetric flow rate, m^3/s

* Mechanical Engineering Co-op, AFRL/PRPS, 1950 Fifth St. Member AIAA.
† Research Engineer, AFRL/PRP, 1950 Fifth St. Senior Member AIAA.
‡ Associate Mechanical Engineer, AFRL/PRPS, 1950 Fifth St. Member AIAA.
§ Associate Professor, Department of Mechanical and Materials Engineering. Associate Fellow AIAA.

$\bar{x}$ = distance from bottom surface of heater conductive layer, m
ρ = density, kg/m^3

Subscripts
air = air
b = bottom of the heater conductive layer
CHF = critical heat flux
cov = heater glass cover plate
FC = FC-72 fluid
htr = heater conductive layer
int = interface between heater substrate and insulating support post
m = measured
s = heater surface
sat = saturation conditions
sc = subcooling
sub = heater ceramic substrate
t = top of the heater conductive layer
∞ = freestream value

I. Introduction

IN the world of power electronics, it has become necessary to find efficient and effective modes of waste heat removal. Spray cooling has been determined to be an effective application for use with delicate electronic equipment because it takes advantage of the latent heat of vaporization as well as the forced convective nature of the liquid spray. It has been noted that the heat transfer associated with spray cooling is affected by the amount of dissolved air present in the cooling fluid. Although research has been conducted concerning this topic, the effect of dissolved air on spray cooling efficiency has not been completely characterized.

The effect of dissolved air on spray cooling, with water as the working fluid, was investigated by Milke et al. (1997). A solid plate of Macor, a glass-like material, was heated using radiant heaters, and spray cooled using a droplet dispenser positioned vertically over the tile. The ratio of the surface temperature change to a reference temperature was examined for air-saturated and degassed water spray cooling application. The actual amount of dissolved air in the fluid was not calculated or measured. For large ratios, the air-saturated and degassed water had similar cooling effects on the heated surface. For smaller ratios, however, it was observed that dissolved gases in the water enhanced cooling by reducing the radiant input.

Pool boiling using FC-72 as the working fluid has also been investigated. Rainey et al. (2003) studied the effects of pressure, subcooling, and dissolved gas on the pool boiling heat transfer performance of a microporous enhanced surface and a plain reference surface, and developed correlations for nucleate boiling and CHF. The results of the experiment suggested that dissolved air contained within FC-72 caused an increase in heat transfer at low heat fluxes just after the onset of superheat, but not at higher heat fluxes. Air-saturation was not seen to have a direct effect on CHF in pool boiling. Test cases were run using air saturated and completely degassed liquid. Tests were not run using intermediate values of dissolved air, and the amount of dissolved air was not directly calculated or measured.

The effect of noncondensible gas on spray cooling, with FC-72, was addressed by Lin et al. (2003). A multi-nozzle array was used to investigate thermal performance data for varying fluids, operating temperatures, nozzle pressure drops, and heat fluxes. The CHF was observed to increase with an increase in dissolved gas content of the FC-72 spray. However, the mass flux onto the heater surface also increased, indicating that both the increase in dissolved gas and mass flux played a role in the observed increase in CHF. The amount of dissolved gas was not directly measured or calculated.

Some work has been done involving the overall spray cooling efficiency of FC-72 with variation in amounts of dissolved air. Horacek et al. (2003) investigated the effect of dissolved gas on spray cooling heat transfer using a full cone Isothermal Systems Research spray nozzle and microheater array. Five cases were conducted involving variation of gas content and thermal subcooling in the working fluid, and pressure. The presence of gas in the FC-72 was seen to increase the spray cooling efficiency overall, when the five cases were compared. Henry's law was used to calculate the amount of dissolved gas via partial pressure; however, no direct measurement was performed.

Further work was done by Horacek et al. (2004) to investigate the effect of dissolved gases on spray cooling heat transfer using measurements of time and space resolved heat transfer distribution and measurements of the liquid-solid contact area and three-phase contact line length using a total internal reflectance technique. Five test cases

were run, involving varying levels of gas and thermal subcooling. The results from the experiment indicated that the gas saturated cooling fluid caused a shift in the saturation temperature of the fluid. As a result, the subcooling of the fluid was also increased, causing an increase in heat transfer. As in the previous work, partial pressures were used to calculate the amount of dissolved gas in the liquid.

The objective of the present investigation was to determine the effect of absorbed air on critical heat flux with FC-72 as the working fluid while controlling the spray chamber pressure. Because amounts of air as large as 48% by volume can be dissolved in FC-72, an understanding of the effect of dissolved air on surface heat flux is critical to understanding the general effectiveness of spray cooling using FC-72. For the experiment, data was collected over a range of volume-percent air content, approximately $1 < C < 20\%$. Each data set contained test runs at flow rates of $\dot{V} = 6.31\times10^{-6}$, 8.41×10^{-6}, and 10.5×10^{-6} m^3/s (6.0, 8.0, and 10.0 gph), a specified air content by volume, C, chamber saturation pressure, P_{sat}, and fluid subcooling, ΔT_{sc}. The percentage air by volume in the FC-72 was measured directly, then corrected for experimental conditions using a ratio of partial pressures. An empirical mathematical model was also developed, relating surface heat flux to volumetric flow rate, subcooling, sensible heat, and CHF.

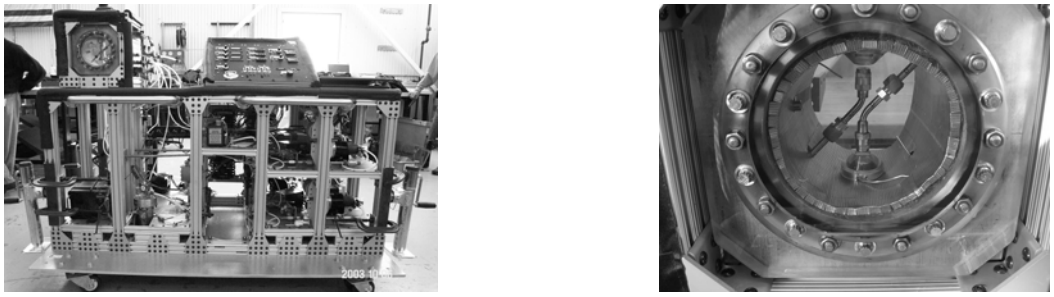

a) **b)**

Figure 1. Experimental test rig showing the: (*a*) complete package and (*b*) test chamber.

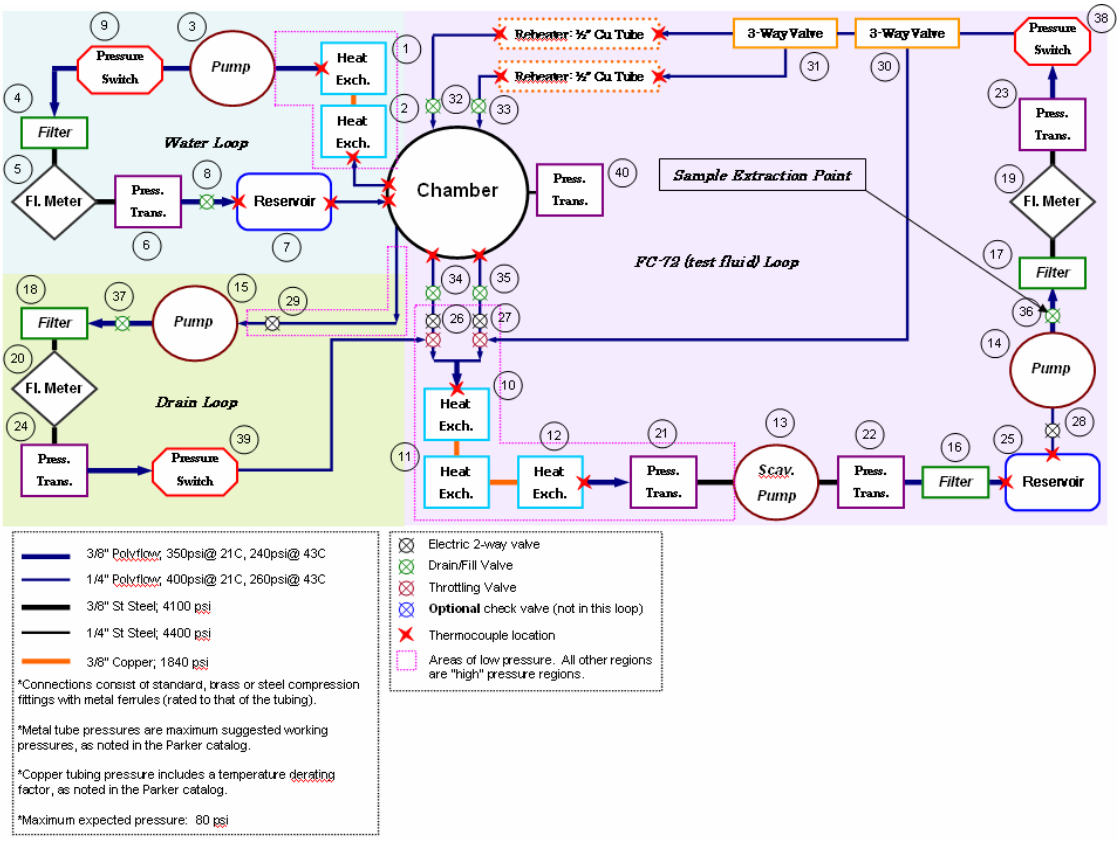

Figure 2. Flow loop schematic for the experimental test rig.

II. Experimental Design and Test Procedure

The test rig used for experimentation was very similar to that described by Baysinger et al.[1,2,3] A spray chamber coupled to a fluid delivery loop system made up the two main components of the test rig. A view of the entire test rig can be seen in Fig. 1(a), while a close-up of the chamber can be seen in Fig. 1(b). Within the spray chamber, two opposing nozzles allowed fluid to be sprayed onto two opposing thick-film resistor heaters. The heaters were mounted on glass posts, and a sump system was used to remove excess fluid. During testing, temperature data was taken using thermocouples imbedded within the heater pedestal. For the current experiment, only the bottom nozzle was used.

The fluid recirculation system consists of two loops. One fluid loop contains the Fluorinert liquid cooling fluid, FC-72, which circulates through the loop and is sprayed from the nozzle onto the heater surface during testing. The second fluid loop contains water, which circulates around the chamber to control the saturation temperature and pressure of the FC-72. Flow rate is controlled using pumps, valves, and reservoirs. The system was monitored using a data acquisition system, flow meters, pressure transducers, and type E thermocouples. A flow schematic can be seen in Fig. 2.

The heater used in the experiment consists of a ceramic substrate, a thick film resistive element, and a glass cover plate. The thicknesses and thermal conductivities of these materials can be seen in Table 1. The ceramic substrate forms the base of the heater, while the glass cover plate protects the resistive element. The entire heater element is attached to the glass post using optical cement.

Layer	Thickness (m)	Thermal Conductivity (W / m-K)
Substrate	$H_{sub} = 0.000634$	$k_{sub} = 27.0$
Heater	$H_{htr} = 0.000008$	$k_{htr} = 1.04$
Cover	$H_{cov} = 0.000040$	$k_{cov} = 1.04$

Table 1. Heater layer characteristics.

To control the amount of air contained within the FC-72 at any given time, a Membrana Superphobic membrane filter, Model G628, was used. The filter consists of a plastic cylinder with an internal membrane permeable to air, but impermeable to FC-72. Three fittings are incorporated into the filter: One to which a vacuum pump can be attached, and two others which allow the working fluid to pass from the rig, through the filter and return to the rig. As the fluid flows through the filter, air is removed. The chamber pressure was used as a rough indicator of the amount of air in the system at any given time. The filter can be seen in Fig. 3.

Figure 3. Membrane filter.

Before each test run, a sample of FC-72 was taken and tested for air content using a Seaton-Wilson AD-4003 Aire-ometer, which can be seen in Fig. 4. These samples were extracted through the fill valves downstream of the reservoir. To keep any non-system air from being introduced to the sample, the sample line was purged of air and replaced with working fluid. Each sample was then pressure-fed to a hypodermic syringe consisting of approximately five milliliters of fluid. The sample volume was less than 1% of the total fill volume of the spray system. During analysis, one milliliter of the sample was used to flush the Aire-ometer liquid line. A 1-ml sample was then placed in the Aire-ometer tube, and the fluid contained within the tube was placed under a slight vacuum, separating the gas contained within the fluid from the fluid itself. This process was repeated three times for each subsequent 1-ml sample, and a reading was taken. Three 1-ml samples were analyzed, at a given each air content condition, to ensure accuracy.

Figure 4. Aire-ometer used for measuring dissolved gas in fluids.

The chamber saturation pressure, $P_{sat,}$ was controlled and adjusted if necessary using a reheater incorporated into the water loop. A reheater incorporated into the FC-72 loop was used to raise the nozzle temperature to achieve the desired amount of fluid subcooling. Once the system was determined to be in equilibrium, the test was started. Tests were conducted by supplying voltage to the thick film resistor heater starting at Q = 5 W and incrementing the heat input by 5 W every 2 minutes, allowing the system to reach steady state at each heater increment. For data evaluation purposes, Q_{CHF} was defined to be 2.5 W less than the heater power load at which CHF appeared to occur. Such a method for determination of Q_{CHF} was developed to account for the fact that the actual power which tripped CHF may have occurred at a level lower than the final power setting, but higher than the previous power setting. Once CHF was reached, the heater power was turned off and the test was finished. Figure 5 shows a typical experimental surface temperature trace with time.

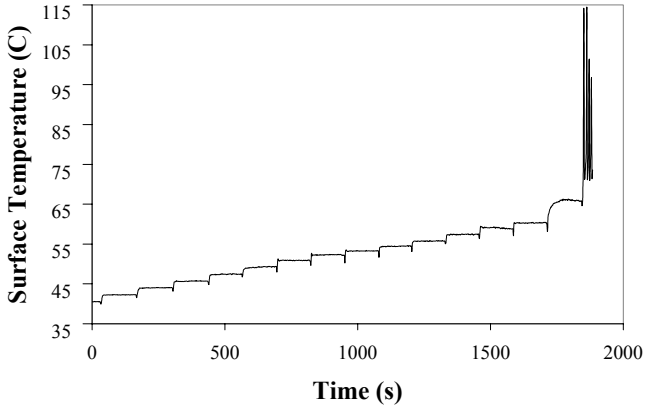

Figure 5. Temperature variation with time.

III. Mathematical Model

Prior to data reduction, a method for calculation of heater surface temperature was developed. The geometry of the thick film resistor (TFR) heater, along with the heat transfer through the substrate and cover can be seen in Fig. 6.

In the figure, the power produced by the resistive heater is denoted by Q, while f is the fraction of heat lost down the pedestal (assumed to be 1.5%, as in previous papers[1,2,3]). The dashed line included in the figure represents the temperature distribution through the TFR heater. The analysis is based on one-dimensional heat transfer through the heater.

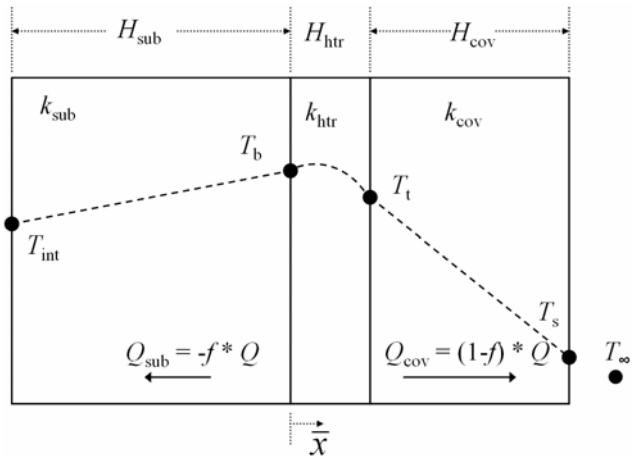

Figure 6. Thick film resistor heater schematic (not to scale).

For the purposes of data reduction, the heater power, Q, and the temperature at the interface between the substrate and the glass pedestal, T_{int}, are known. The temperature profiles in the substrate and cover regions are assumed to be adequately approximated by one-dimensional heat conduction, and the only relevant temperatures for such a case are those at the interfaces. Said temperatures can be obtained using the following equations:

$$Q_{sub} = -k_{sub} A \left(\frac{T_b - T_{int}}{H_{sub}} \right) \Rightarrow \frac{dT}{dx} = \frac{T_b - T_{int}}{H_{sub}} = -\frac{Q_{sub}}{k_{sub} A} \tag{1}$$

$$Q_{cov} = -k_{cov} A \left(\frac{T_s - T_t}{H_{cov}} \right) \Rightarrow \frac{dT}{dx} = \frac{T_s - T_t}{H_{cov}} = -\frac{Q_{cov}}{k_{cov} A} \tag{2}$$

T_b, the temperature between the substrate and the heater, can be calculated as:

$$T_b = -\frac{Q_{sub} H_{sub}}{A k_{sub}} + T_{int} = -\frac{f Q H_{sub}}{A k_{sub}} + T_{int} \tag{3}$$

The temperature distribution within the heater is assumed to be a parabolic function in terms of $\bar{x}$ shown on the schematic. The parabolic temperature must have temperatures and slopes on either side of the vertex consistent with those determined by the heat transfer through the substrate and cover:

$$T(\bar{x}) = \bar{A}\bar{x}^2 + \bar{B}\bar{x} + \bar{C};\ 0 \le \bar{x} \le H_{htr} \tag{4}$$

$$\bar{x} = 0,\ T(0) = T_b \tag{5}$$

$$\bar{x} = 0,\ \frac{dT}{d\bar{x}} = -\frac{Q_{sub}}{A k_{sub}} \tag{6}$$

$$\bar{x} = H_{htr},\ \frac{dT}{d\bar{x}} = -\frac{Q_{cov}}{A k_{cov}} \tag{7}$$

$$\bar{x} = H_{htr},\ T(H_{htr}) = T_t \tag{8}$$

Using the first three boundary conditions (BC) to solve for the unknown constants $\bar{A}, \bar{B}, \bar{C}$ and substituting these into the distribution gives:

$$T(\bar{x}) = \frac{1}{2AH_{htr}}\left(\frac{Q_{sub}}{k_{sub}} - \frac{Q_{cov}}{k_{cov}}\right)\bar{x}^2 - \frac{Q_{sub}}{A k_{sub}}\bar{x} + T_b \tag{9}$$

Now, $\bar{x} = H_{htr}$ (fourth BC) is substituted to obtain the value for T_t, the temperature at the interface between the heater layer and the glass cover:

$$T_t = \frac{1}{2AH_{htr}}\left(\frac{Q_{sub}}{k_{sub}} - \frac{Q_{cov}}{k_{cov}}\right)(H_{htr})^2 - \frac{Q_{sub} H_{htr}}{A k_{sub}} + T_b \tag{10}$$

The temperature at the surface of the glass cover can be given as:

$$T_s = T_t - \frac{Q_{cov} H_{cov}}{A k_{cov}} = T_t - \frac{(1-f) Q H_{cov}}{A k_{cov}} \tag{11}$$

Now, substituting the value of T_t given above and simplifying gives the surface temperature as:

$$T_s = T_b + \frac{Q H_{htr}}{A}\left\{\frac{f}{k_{sub}} - \frac{1}{2}\left[\frac{f}{k_{sub}} + \frac{(1-f)}{k_{cov}}\right]\right\} - \frac{(1-f) Q H_{cov}}{A k_{cov}} \tag{12}$$

The surface temperature from Eqn. 12 was used for data reduction purposes.

An empirical mathematical model was also developed to take into account subcooling, sensible heat, CHF, and volumetric flow rate. Heat flux was plotted as a function of the temperature drop from the surface of the heater to the saturation temperature, $\Delta T = T_s - T_{sat}$. A second-order mathematical relationship allowing determination of surface heat flux for a given flow rate and surface temperature was developed, as shown in Fig. 7.

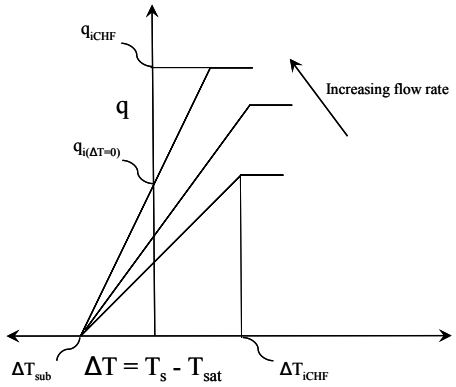

Figure 7. Surface heat flux vs ΔT points of interest.

a)

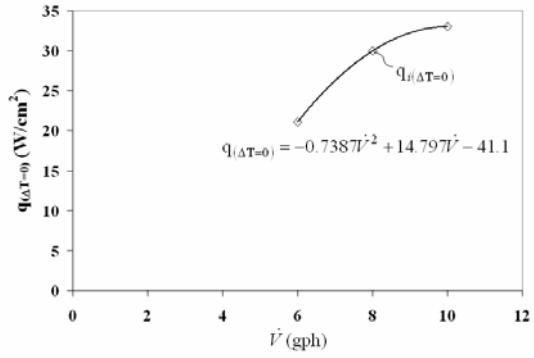

b)

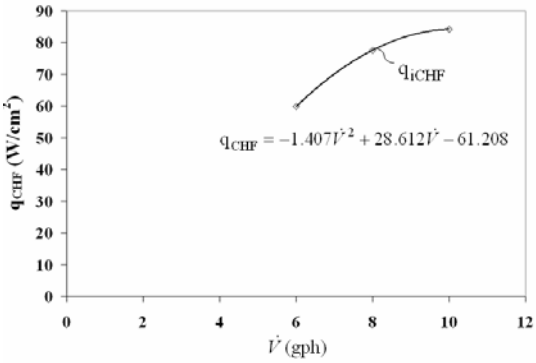

c)

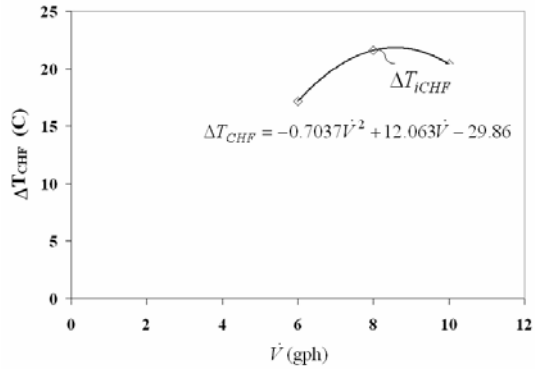

Figure 8. Functional relationship equations for: (a) $q_{(\Delta T=0)}$, (b) q_{CHF}, and (c) ΔT_{CHF}.

Considering the surface heat flux, q, as a function of ΔT of the form $q = a\Delta T^2 + b\Delta T + c$, the coefficients *a,b,* and *c* can be derived from ΔT_{sc} and three functional relationships, with the volumetric flow rate, $\dot{V}$. The functional relationships are those for $q_{(\Delta T=0)}$, the sensible heat, q_{CHF}, the critical heat flux, and ΔT_{CHF}, the ΔT at which critical heat flux occurs.

To obtain functional relationships for $q_{(\Delta T=0)}$, q_{CHF}, and ΔT_{CHF}, each variable was plotted against flow rate using experimental data at three different values for $\dot{V}$. A second-order polynomial fit was then used to obtain a functional relationship for each variable with $\dot{V}$. Figure 8 shows the three functional relationships for $q_{(\Delta T=0)}$, q_{CHF}, and ΔT_{CHF} with volumetric flow rate, $\dot{V}$, for the case of C = 10%, $10 \le \Delta T_{sc} \le 12$°C, and $\dot{V} = 6.31\times10^{-6}$, 8.41×10^{-6}, and 10.5×10^{-6} m^3/s (6.0, 8.0, and 10.0 gph).

Following determination of the functional relationships, the coefficients of the general equation are determined. First, the coefficient *c* is determined using $q_{(\Delta T=0)}$:

$$q_{(\Delta T=0)} = a(0)^2 + b(0) + c \tag{13}$$

$$c = q_{(\Delta T=0)} \tag{14}$$

The general equation now becomes

$$q = a\Delta T^2 + b\Delta T + q_{(\Delta T=0)} \tag{15}$$

The coefficients *a* and *b* are then evaluated using the following simultaneous equations:

$$q_{CHF} = a(\Delta T_{CHF})^2 + b(\Delta T_{CHF}) + q_{(\Delta T=0)} \tag{16}$$

and

$$0 = a(\Delta T_{sc})^2 + b(\Delta T_{sc}) + q_{(\Delta T=0)} \tag{17}$$

Following algebraic manipulation, coefficient *a* is determined to be

$$a = -\left\{ \frac{q_{(\Delta T=0)}}{\Delta T_{sc}^2} + \frac{\left[q_{CHF} + \frac{q_{(\Delta T=0)}\Delta T_{CHF}^2}{\Delta T_{sc}^2} - q_{(\Delta T=0)} \right]}{\Delta T_{sc}\left[\Delta T_{CHF} - \frac{\Delta T_{CHF}^2}{\Delta T_{sc}} \right]} \right\} \tag{18}$$

and coefficient *b* becomes

$$b = \left\{ \frac{q_{CHF} + \frac{q_{(\Delta T=0)}\Delta T_{CHF}^2}{\Delta T_{sc}^2} - q_{(\Delta T=0)}}{\left[\Delta T_{CHF} - \frac{\Delta T_{CHF}^2}{\Delta T_{sc}} \right]} \right\} \tag{19}$$

Now, the second-order relationship becomes

$$q = -\left\{ \frac{q_{(\Delta T=0)}}{\Delta T_{sc}^2} + \frac{\left[q_{CHF} + \frac{q_{(\Delta T=0)} \Delta T_{CHF}^2}{\Delta T_{sc}^2} - q_{(\Delta T=0)} \right]}{\Delta T_{sc} \left[\Delta T_{CHF} - \frac{\Delta T_{CHF}^2}{\Delta T_{sc}} \right]} \right\} \Delta T^2 + \left\{ \frac{q_{CHF} + \frac{q_{(\Delta T=0)} \Delta T_{CHF}^2}{\Delta T_{sc}^2} - q_{(\Delta T=0)}}{\left[\Delta T_{CHF} - \frac{\Delta T_{CHF}^2}{\Delta T_{sc}} \right]} \right\} \Delta T + q_{(\Delta T=0)}. \quad (20)$$

The above equation can now be used to predict surface heat flux for varying ΔT for a given $\dot{V}$.

IV. Results and Discussion

Set	Run	$\dot{V}$ *10^6 (m^3/s)	T_{sc} (°C)	T_{sat} (°C)	q_{CHF} (W/cm^2) (± 2.2)	C_m (%) (±2)	C (%)	M
1	a	6.35 ± 0.07	10.0 ± 0.7	41.4 ± 0.4	64.38	8	7.8 ± 2.2	4.26E-05 ± 1.20E-05
	b	6.28 ± 0.06	11.0 ± 0.7	41.2 ± 0.4	62.54	10	10.7 ± 2.4	5.74E-05 ± 1.29E-05
	c	6.28 ± 0.05	11.5 ± 0.7	47.3 ± 0.4	62.83	18	17.1 ± 2.2	1.26E-04 ± 1.65E-05
2	a	8.54 ± 0.13	9.0 ± 1.0	42.3 ± 0.9	69.48	5	1.4 ± 1.1	9.73E-06 ± 8.24E-06
	b	8.51 ± 0.09	9.5 ± 1.0	49.8 ± 0.8	69.34	10	5.4 ± 2.1	5.22E-05 ± 2.13E-05
	c	8.37 ± 0.23	8.5 ± 0.8	50.0 ± 0.4	60.72	16	16.3 ± 2.8	1.52E-04 ± 2.58E-05
3	a	8.79 ± 0.15	12.0 ± 0.9	33.8 ± 0.6	71.64	5	4.4 ± 1.8	1.45E-05 ± 5.95E-06
	b	8.37 ± 0.16	12.0 ± 0.7	42.2 ± 0.5	76.84	10	11.1 ± 2.6	6.53E-05 ± 1.54E-05
	c	8.43 ± 0.09	12.0 ± 0.7	48.7 ± 0.4	76.92	18	17.7 ± 2.4	1.46E-04 ± 2.02E-05
4	a	10.50 ± 0.06	12.0 ± 0.8	42.7 ± 0.5	91.09	8	8.9 ± 2.7	5.56E-05 ± 1.69E-05
	b	10.53 ± 0.11	12.5 ± 0.7	42.9 ± 0.4	90.64	10	11.4 ± 2.8	7.16E-05 ± 1.73E-05
	c	10.53 ± 0.06	13.0 ± 0.7	49.6 ± 0.4	87.35	18	18.1 ± 2.6	1.60E-04 ± 2.28E-05

Table 2. Experimental test run parameters.

Four sets of experimental test runs were made and the results are shown in Table 2. For each data set, control of the spray chamber pressure was used to maintain a specific saturation temperature. Samples of FC-72, to determine the air content, C_m, were taken while the spray chamber was at saturation conditions with an ambient temperature of 20 – 21°C. In this manner, dissolved air in the FC-72 was quantified at specific thermodynamic conditions, but was allowed to vary due to any variation in spray chamber saturation pressure. The measured air content, C_m, was then converted to a volume ratio, C_m^*, and corrected for experimental conditions using Henry's law to give the corrected volume ratio, C^*. This was done by multiplying this volume ratio by the partial pressures and accounting for density changes in the liquid FC-72 and air using the relation

$$C^* = \frac{C_m^* P_g \left(\frac{\rho_{FC}}{\rho_{air}} \right)}{\left(P_g \right)_m \left(\frac{\rho_{FC}}{\rho_{air}} \right)_m}.$$

The corrected volume ratio, C^*, was converted back to a volume fraction, C/100, and is shown as the percent volume, C, in Table 2. In a similar manner, the molar fraction, M_m, was also determined from the volume fraction, C_m/100, converted to a molar ratio, M_m^*, and corrected molar ratio, M^*, was determined using Henry's law by multiplying by the ratio of partial pressures. The corrected molar ratio, M^*, was converted back to a molar fraction, M, and is also shown in Table 2. To evaluate the effect of varying C on critical heat flux, test runs were grouped into four sets of three experimental runs that had statistically comparable $\dot{V}$, ΔT_{sc} and T_{sat}. These four sets of experimental test runs were then compared. Experimental data showing heat flux curves for each of the data sets in Table 2 can also be seen in Figure 9.

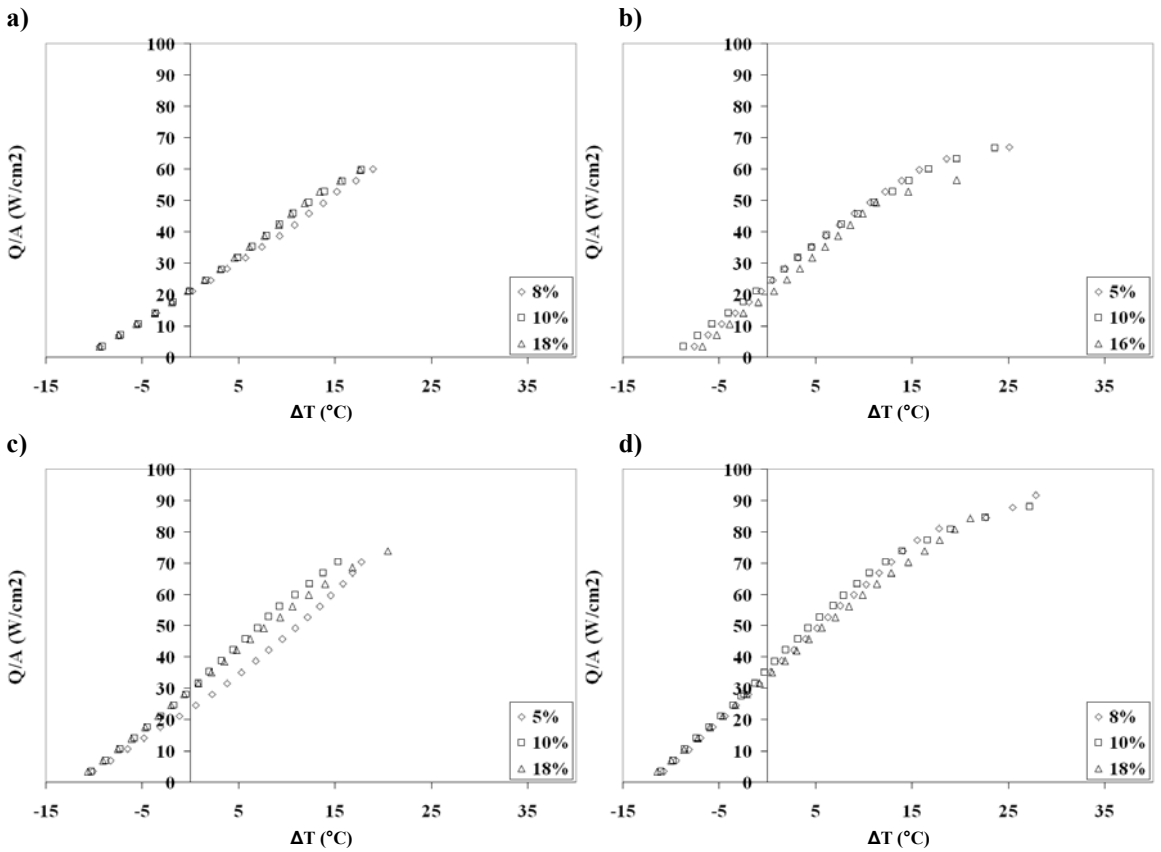

Figure 9. Experimental results showing heat flux versus ΔT for: (a) Set 1, (b) Set 2, (c) Set 3, and (d) Set 4.

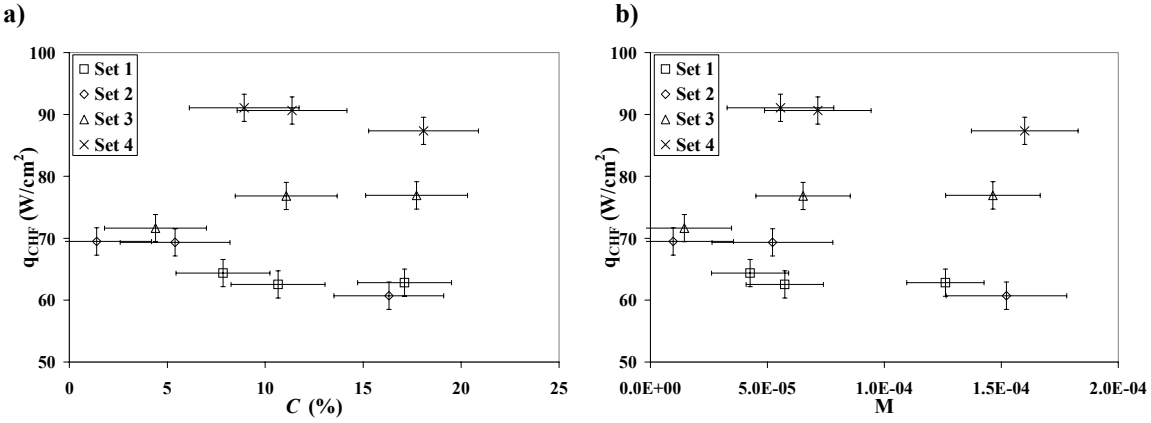

Figure 10. Critical heat flux (CHF) with varying air content for: (a) volume-percent and (b) molar fraction.

In general, there was no significant variation of CHF with *C* as shown in Table 2 and Fig. 10. An exception to this can be seen in Set 3. For this case, there appeared to be a slight increase in CHF with increasing air content. For Run 3a, the saturation temperature was lower, in absence of thermal control of the chamber pressure, resulting in a reduced CHF. This result is consistent with the findings of Horacek et al. (2003) and Lin et al. (2003). However, this was not the case for Run 2a. For this case, the saturation temperature was also lower. However, the amount of dissolved air in Runs 2a and 2b was also low, on the order of <5-6%.

Subcooling also contributed to a variation in CHF as shown in Runs 2c and 3c. For these cases, both had air content within experimental uncertainty, 17.7% and 18.1% respectively, but due to an increase in subcooling, the CHF was greater for Run 3c than for Run 2c. The effect of subcooling was not as noticeable at the lower air

content, 4-5%, as shown in Runs 2b and 3a. Also noted was the increase in CHF with flow rate for Sets 1, 2 & 3, and 4. Run 2c showed a decrease in CHF most likely due to the lower flow rate accompanied with a larger than usual uncertainty. These results are also consistent with prior investigations.

The proposed empirical mathematical model was evaluated through comparison of experimental data and predicted data using Eqn. 20. The model was evaluated for Runs 1b, 3b, and 4b where C_m = 10%, $10 \le \Delta T_{sc} \le 12$°C, and $\dot{V} = 6.31\times10^{-6}$, 8.41×10^{-6}, and 10.5×10^{-6} m^3/s (6.0, 8.0, and 10.0 gph). Functional relationships were obtained by the method previously discussed. The coefficients were then determined, and Eqn. 20 was used to predict the behavior of surface heat flux at $\dot{V} = 7.36\times10^{-6}$ and 9.46×10^{-6} m^3/s (7.0 and 9.0 gph). The experimental and analytical results were plotted and compared. Figure 11 shows these results including those for the original flow rates of $\dot{V} = 6.31\times10^{-6}$, 8.41×10^{-6}, and 10.5×10^{-6} m^3/s (6.0, 8.0, and 10.0 gph), from which Eqn. 8 was derived. In Figure 11, experimental data is depicted using isolated points, while analytical data is depicted using solid lines. As can be seen in the plot, the predicted heat flux compares very well with the experimental data obtained for both flow rates.

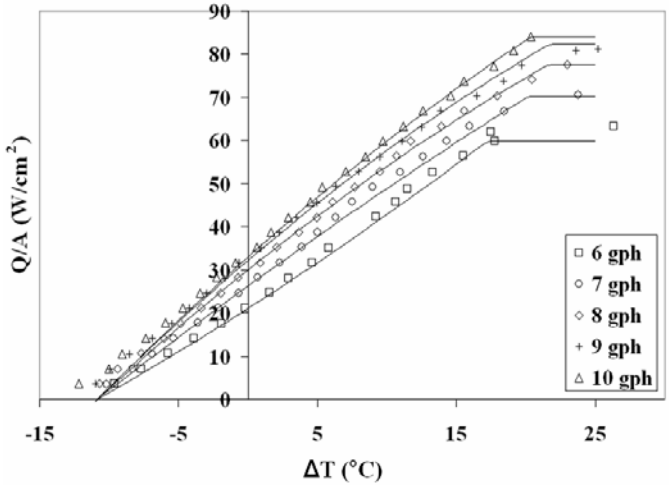

Figure 11. Mathematical fit with experimental data included.

V. Conclusions

The effect of dissolved air on the heat transfer of a partially-confined spray was investigated for $1 < C < 20\%$. An empirical mathematical model correlating flow rate, subcooling, sensible heat, and critical heat flux using experimental data was also presented. For the most part, there was no significant variation in heat transfer performance due to varying dissolved air in the spray system when the pressure of the spray chamber was thermally controlled to maintain a saturation temperature. This was not the case if the system, containing dissolved air, and was allowed to come to thermodynamic equilibrium without thermally controlling the chamber pressure. The exception to this was the case where the dissolved air was relatively low, $C<5\%$. The empirical mathematical model was used to predict the behavior of two test runs and agreed well with experimental data. This may provide a useful, reduced order, empirical approach that could be used to model spray cooling components imbedded into system level thermal management models.

Acknowledgments

This research was conducted as part of the in-house program at the Air Force Research Laboratory, Propulsion Directorate, Power Division, Electrochemistry and Thermal Sciences Branch, AFRL/PRPS, Wright-Patterson Air Force Base, Ohio.

References

[1]Baysinger, K. M., Yerkes, K. L., Michalak, T. E., Harris, R. J., and McQuillen, J., "Design of a Microgravity Spray Cooling Experiment," *Proc. 42nd AIAA Aerospace Sciences Conference and Exhibit*, Paper No. AIAA-2004-0966, 2004.

[2]Baysinger, K. M., Yerkes, K. L., and Thomas, S. K., "Experimental Testing and Numerical Modeling of Spray Cooling Under Terrestrial Gravity Conditions," AFRL-PR-WP-TR-2005-2047, 2005.

[3]Baysinger, K. M., "Experimental Testing and Numerical Modeling of Spray Cooling Under Terrestrial Gravity Conditions," Masters Thesis, Wright State University, Department of Mechanical and Materials Engineering, 2005.

[4]Horacek, B., Kim, J., and Kiger, K. T., "Effects of Noncondensable Gas and Subcooling on the Spray Cooling of an Isothermal Surface," *Proc. ASME IMECE,* Paper No. IMECE-2003-41680, 2003.

[5]Horacek, B., Kim, J., and Kiger, K. T., "Gas Effects on Spray Cooling of an Isothermal Surface: Visualization and Time and Space Resolved Heat Transfer Measurements," *Proc. 42nd AIAA Aerospace Sciences Meeting and Exhibit,* Paper No. AIAA-2004-1345, 2004.

[6]Lin, L., and Ponnappan, R., "Heat Transfer Characteristics of Spray Cooling in a Closed Loop," *Intl. J. Heat Mass Transfer,* Vol. 46, 2003, pp. 3737-3746.

[7]Milke, J. A., Tinker, S. C., and diMarzo, M., "Effect of Dissolved Gases on Spray Evaporative Cooling with Water," *Fire Technology,* 2nd Quarter, Vol. 33, No. 2, 1997, pp. 99-113.

[8]Rainey, K. N., You, S. M., and Lee, S., "Effect of Pressure, Subcooling, and Dissolved Gas on Pool Boiling Heat Transfer from Microporous Surfaces in FC-72," *ASME J. Heat Transfer,* Vol. 125, 2003, pp. 75-83.